Active spectroscopy measurements of the deuterium temperature, rotation, and density from the core to scrape off layer on the DIII-D tokamak[a)]

S. R. Haskey,[1, b)] B. A. Grierson,[1] L. Stagner,[2] C. Chrystal,[3] A. Ashourvan,[1] A. Bortolon,[1] M. D. Boyer,[1] K. H. Burrell,[3] C. Collins,[3] R. J. Groebner,[3] D. H. Kaplan,[3] and N. A. Pablant[1]

[1)] *Princeton Plasma Physics Laboratory, Princeton, New Jersey 08543-0451, USA*

[2)] *University of California, Irvine, California 92697, USA*

[3)] *General Atomics, PO Box 85608, San Diego, CA 92186, USA*

(Dated: 1 October 2018)

Main-ion charge exchange recombination spectroscopy (MICER) uses the neutral beam induced D_α spectrum to measure local deuterium ion (D^+) temperature, rotation, and density, as well as parameters related to the neutral beams, fast ions, and magnetic field. An edge MICER system consisting of 16 densely packed chords was recently installed on DIII-D extending the MICER technique from the core to the pedestal and steep gradient region of H-mode plasmas where the D^+ and commonly measured impurity ion properties can differ significantly. A combination of iterative collisional radiative modeling techniques and greatly accelerated spectral fitting allowed the extension of this diagnostic technique to the plasma edge where the steep gradients introduce significant diagnostic challenges. The importance of including the fast ion D_α emission in the fit to the spectrum for the edge system is investigated showing that it is typically not important except for cases which can have significant fast ion fractions near the plasma edge such as QH-mode. Example profiles from an Ohmic L-mode and a high power ITER baseline case show large differences in the toroidal rotation of the two species near the separatrix including a strong co-current D^+ edge rotation. The measurements and analysis demonstrate the state of the art in active spectroscopy and integrated modeling for diagnosing fusion plasmas and the importance of direct main ion measurements.

I. INTRODUCTION

The main ion (typically deuterium) temperature, toroidal rotation, and density profiles are required for testing transport models and improving predictive capabilities in magnetic confinement devices. The main ion temperature is one of the key parameters of a fusion relevant plasma and the toroidal rotation and its shear can play a crucial role in determining stability to large scale MHD, $\mathbf{E} \times \mathbf{B}$ shear stabilization of micro-turbulence[1], and access to advanced operating scenarios such as ELM suppressed H-mode and QH mode[2].

Typically, impurity charge exchange recombination spectroscopy (CER)[3–5] is used to determine the temperature, rotation, and density of an impurity species using the Doppler broadening, Doppler shift, and radiance of spectral emission from an impurity species. On DIII-D the C-VI (n = 8 → 7, 5290.5Å) transition is usually used with measurements available between discharges or in realtime for control purposes. While these measurements are accurate and have a high availability, the difficulty comes from relating the impurity properties to those of the main ions with the typical approach being to assume they are equal or to use neoclassical models to infer the main ion properties. This can lead to erroneous inferred main ion properties. For example, the main ion and impurity toroidal rotation are known to diverge considerably in low collisionality conditions[6,7] and in regions where there are steep pressure gradients such as the pedestal region, providing a significant modeling challenge that requires high resolution experimental data for validation.

An alternative to impurity CER is to use spectral emission from the main ions to determine their properties directly. Early work on T-10[8], TEXTOR[9], and JET[10] demonstrated that the measurement was possible using D_α emission (D-I [n = 3 → 2, 6561.0Å]) due to charge exchange with the neutral beams as well as the associated halo emission; however, due to a more complex spectrum with several features including a bright cold edge D_α feature, cross section distortions and halo emission, the use and development of this diagnostic technique was limited until recently. Advances in main ion CER spectroscopy (MICER) have allowed accurate direct measurements of the deuterium ion properties in the plasma core[11] and more recently the pedestal and steep gradient region[12–14] in deuterium beam heated plasmas on DIII-D to become more common. In addition there has been recent work in this field on AUG[15] and T-10[16].

Main ion measurements have also been made in helium plasmas using CER with deuterium NBI[17,18]; however, these plasmas suffer from deuterium dilution and are rarely created due to operational overhead. Bulk plasma rotation measurements can also be made using Mach probes[19]; however due to power flux considerations, these measurements are limited in duration, scenario, and depth into the plasma. Additionally collective Thomson scattering is another promising approach for determining the temperature and rotation of the main

[a)] Invited paper published as part of the Proceedings of the 22nd Topical Conference on High-Temperature Plasma Diagnostics, San Diego, California, April, 2018.

[b)] Electronic mail: shaskey@pppl.gov

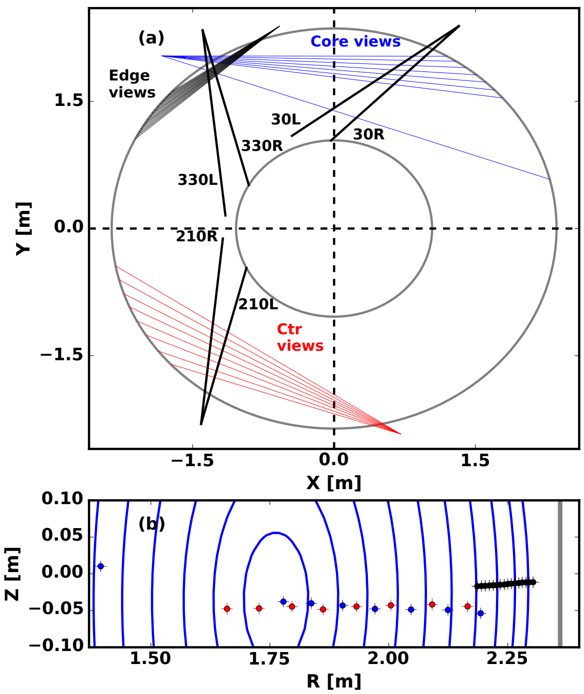

FIG. 1. (a) Midplane plan view of DIII-D showing the location of the beam lines that the main ion system views (30L, 30R, 330L, 330R, 210L, 210R) and the three main ion systems. (b) Midplane poloidal cross section showing the locations of the views based on their intersection with 30L (core), 330L (edge), and 210L (counter) respectively along with equilibrium flux surfaces from the ITER baseline case. More details in text.

ion species[20].

This paper describes some key elements of MICER as well as recent advances which have enabled core to scrape off layer main ion measurements, particularly in the areas of spectral fitting and atomic physics related corrections. Data from three different discharges with very different parameters are shown in this paper. A low power Ohmic L-mode discharge (#173147) which was used to study intrinsic rotation, a high performance 0 $\mathrm{N \cdot m}$ torque ITER baseline scenario H-mode (#164988), and a high power, high temperature, low density QH-mode (#169366). These discharges span a wide range of temperatures, rotations, and fast ion fractions, representing a significant range of parameters achievable on DIII-D. These cases are referred to as the Ohmic case, the ITER baseline case, and the QH-mode case in the remainder of this paper.

II. THE DIII-D MICER SYSTEM

The MICER system on DIII-D is a dedicated spectroscopic system consisting of 32 channels grouped into three sub-systems. Some key details of the systems are included here – the reader is referred to Refs. 12 and 11 for more details on the edge and core systems respectively. In addition, impurity CER has been used on DIII-D since its initial operation and includes a recently expanded high resolution edge system[21] with sight lines which are interleaved with the edge main ion system allowing straight forward comparisons between the impurities and main ions.

A plan view of the channel locations and associated NBI systems is shown in Fig. 1. The main ion CER system views six of the eight NBI beamlines on DIII-D. Each beamline is labeled by the toroidal angle of the injection port (30, 210, 330) and a letter (L or R) to identify the two beamlines at each port. There are two core main ion systems with eight channels each viewing neutral beam injectors directed in opposite toroidal directions (blue and red in Fig. 1) and a sixteen channel high resolution edge system (black in Fig. 1). One of the core chords is located significantly on the high field side for exploratory purposes. Each channel of the edge (core) system consists of pairs of 750 μm (single 1500 μm) core diameter fibers. For the edge system the pairs of fibers are stacked vertically (see Fig 1. in Ref. 12) to improve signal without reducing radial resolution. All systems use scanning Czerny-Turner 2/3 m McPherson model #207 spectrometers and the spectra are acquired using SRI Avanti-768 CCD cameras which have a 768 x 256 grid of 18 μm $\times$ 18 μm pixels. The reciprocal dispersion is typically 0.18 Å/pixel with a full spectral width of 138 Å. In total there are four spectrometers with eight channels and two cameras per spectrometer.

High speed operation at integration times down to 0.128 ms is possible; however, for typical operation the integration times are 5 ms. In order to avoid saturation due to the bright cold D_α line (particularly in ELMing plasmas), this 5 ms integration time is typically divided into between 2 and 10 shorter acquisitions which are binned in software.

III. MICER ANALYSIS

The measurement and acquisition of the emission spectra for the impurity and main ion systems on DIII-D are almost identical; however, MICER analysis is usually substantially more involved than impurity CER due to the existence of more features in the D_α spectrum and the extensive calculations required to correct for cross section distortions and halo related spatial smearing. While this is a computationally intensive and time consuming process, the D_α spectrum provides measurements beyond impurity CER including neutral beam related measurements such as beam velocity, radiance of the full, half, and third, energy components, magnetic field strength (through Stark splitting), and information on the fast ion population through fast ion D_α (FIDA)[22].

The typical workflow for analyzing MICER data on

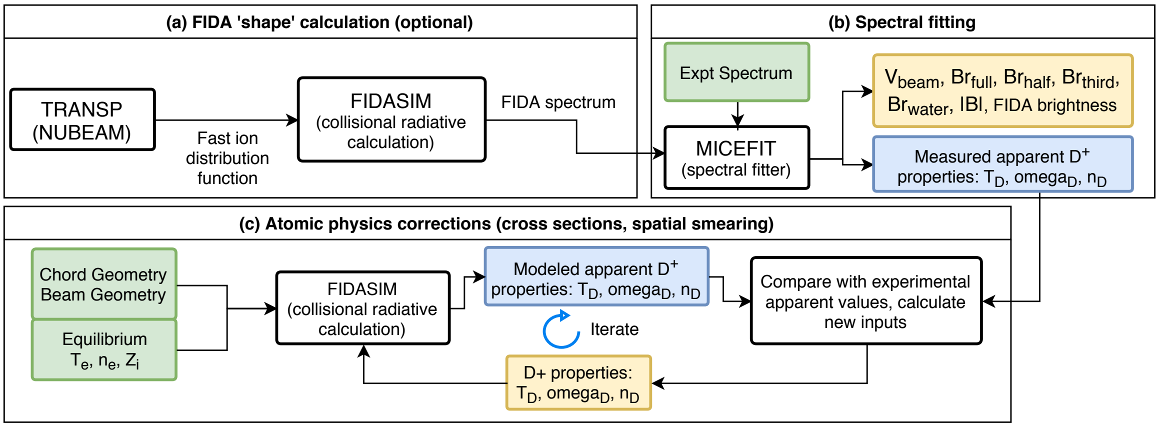

FIG. 2. The typical workflow for analyzing MICER data on DIII-D. (a) FIDASIM is used to calculate the FIDA spectrum for each sight-line using the TRANSP calculated fast ion distribution function (section III D). (b) A model is fit to the measured spectra (section III A). (c) An iterative collisional radiative modeling scheme is used to correct the apparent measurements (section III C).

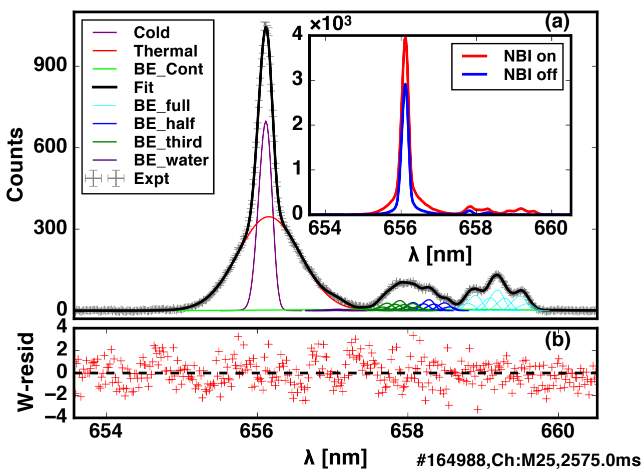

FIG. 3. (a) Background subtracted spectrum and fit to the spectrum with the NBI on and NBI off spectra inset. (b) Residual from the fit weighted by the uncertainty of the measured spectrum at each pixel based on photon statistics, dark noise, and readout noise.

DIII-D is shown in Fig. 2 and usually involves three broad steps: (a) calculating the fast ion D_α (FIDA) spectrum based on the fast ion distribution function from TRANSP (see section III D), (b) using beam on - beam off timeslice subtraction to isolate the active emission and fitting a comprehensive model to the resulting spectrum, and (c) calculating the corrections due to cross section distortions and the halo using an iterative collisional radiative approach which is described briefly in section III C and in substantially more detail in Ref. 14. A great deal of progress has been made accelerating the various steps, in particular the spectral fitting, although an overall goal of being able to perform automated main ion analysis between discharges has yet to be achieved.

A. Fitting the D_α Spectrum

A typical spectrum for an edge chord for the high performance ITER baseline case in H-mode is shown in Fig. 3 using active-passive time slice subtraction (see section III B for more details). The fit model includes the following features: a thermal feature (constrained to have a minimum temperature of 80 eV) which carries information about the main ion properties, a residual cold feature (constrained to have a temperature below 20 eV), impurity lines, fast ion D_α (FIDA), and beam related emission. The beam emission consists of a full (D^+), half (D_2^+), third (D_3^+), and water (D_2O^+) component each of which is accelerated to a different velocity due to their different mass before breaking apart in the neutralizer. Additionally there is broad continuum feature thought to be due to the breakup of D^{2+}, D^{3+}, and D_2O^+ in the accelerator[23]. The location of this feature is fixed relative to the full energy feature, the radiance is tied to third energy radiance, and the width is constrained such that the emission is essentially zero when the velocity reaches the velocity of the beam water emission and the full energy emission. The location, profile, and relative radiance of the continuum feature are determined using beam into gas calibration shots. Additionally, sometimes a cold H_α feature is included if there is significant hydrogen present (see Fig. 5 for example); however, this is rarely required on DIII-D. For some additional information on how each of these components is constrained for the core and edge systems see Refs. 7 and 12.

The amplitude of the residual cold feature is negligible for the core chords, increases for the edge chords with tangency radii near the separatrix and decreases for chords with tangency in the scrape off layer. This residual feature was unexpected and its origin is currently under investigation. Some possibilities include impact excitation of the cold edge neutrals by beam neutrals and/or fast ions, an increase in the cold neutral density while the beams are on, or changes in the electron impact excitation due to changes in the plasma geometry (caused by increasing plasma beta when the beams are on) which causes the electron density profile to move relative to the neutral density profile.

In order to deal with the high throughput required for more routine analysis a new spectral fitter was written using the C programming language to optimize the execution speed. The new fitting program, called MICEFIT, retains many of the essential features and models of the original fitting software[23] which was written in IDL. The combination of using a compiled language and the ability to parallelize jobs over chords on a cluster has reduced the average time to fit all of the main ion chords for a discharge by approximately two orders of magnitude allowing all chords to be fit in a few minutes if the FIDA calculations which are discussed in section III D are not required.

B. Active-passive time slice subtraction

In order to isolate the D_α emission due to the NBI we subtract a spectrum from when the NBI is off from a spectrum when it is on (referred to as time slice subtraction). This localizes the measurement to the approximate beam - sight line intersection and is more important for MICER than impurity CER because of larger levels of complicating background emission. Fig. 3 shows an example of the time slice subtracted spectrum along with the NBI on and NBI off spectra.

The passive time slice (NBI off) which is chosen for time slice subtraction is usually the closest available time slice within 20ms which is free from significant changes in the plasma such as ELM activity which can have a dramatic effect on the D_α spectrum. One concern is that the measurement is sensitive to which passive time slice is used. Fig. 4 demonstrates that this is not the case. The temperature and rotation for a chord inside the top of the pedestal (M17) and near the separatrix (M30) give very similar results regardless of whether the passive time slices are constrained to be before the measurement time slice, after the measurement, or the one which is closest in time.

Because the NBIs which are used for the MICER measurements on DIII-D are heating beams, the requirement that the beams be modulated on and off places a significant constraint on the beam programming for experiments. This raises the question of how well the spectrum can be fit without using time slice subtraction. Fig. 4 also shows the result of trying to fit the active spectrum without subtracting a passive time slice. For a chord inside the top of the pedestal (M17), the systematic errors are relatively small at 50 eV and 3 km/s. However, near the separatrix, the systematic error is significantly larger at 100 eV and 15 km/s. This is because it becomes more difficult to separate the thermal feature from the cold and warm passive emission due to the reduced ion temperature (this issue is minimized by using time slice subtraction). Including an additional warm feature in the spectrum whose temperature is constrained to be between 20 eV and 100 eV provides slight improvements for the chord further into the plasma but increases the error for the edge chord.

It is important to note that the error is systematic and the underlying dynamics of the measurements are retained when time slice subtraction is not used. This both demonstrates the importance of time slice subtraction for obtaining the most accurate results possible, but also shows that if errors of 100 eV and 15 km/s at the edge (and less in the core) are acceptable, it is possible to use the active signal without time slice subtraction. In such a situation, occasional periods of beam modulation should be used to verify the quality of measurements against time slice subtracted data.

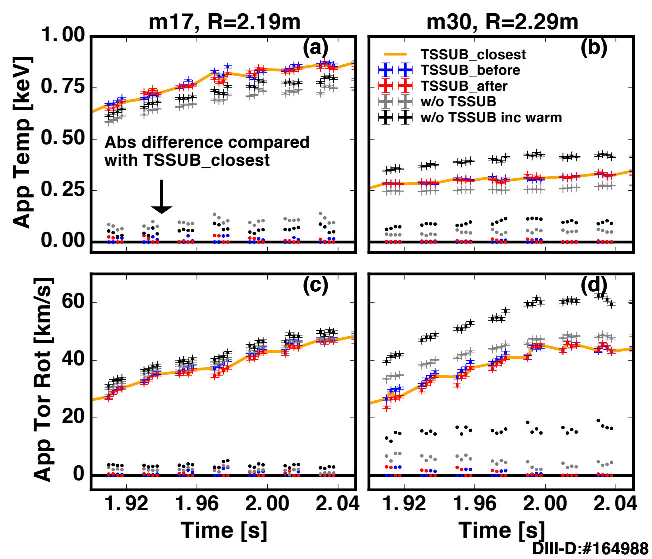

FIG. 4. The result from fitting the spectra with different time slice subtraction (TSSUB) strategies for a chord inside the pedestal top (M17) and near the plasma edge (M30). Using only the timeslices before, after, or closest to the active slice provide very consistent results for both chords. Dots mark the absolute difference compared with the TSSUB closest case. The measurements without using time slice subtraction are shown with and without including an additional warm feature in the fit. Agreement with the TSSUB data is significantly worse for the edge chord.

C. Atomic physics modeling

Fitting the MICER spectrum provides the *apparent* temperature, *apparent* line of sight velocity, and radiance

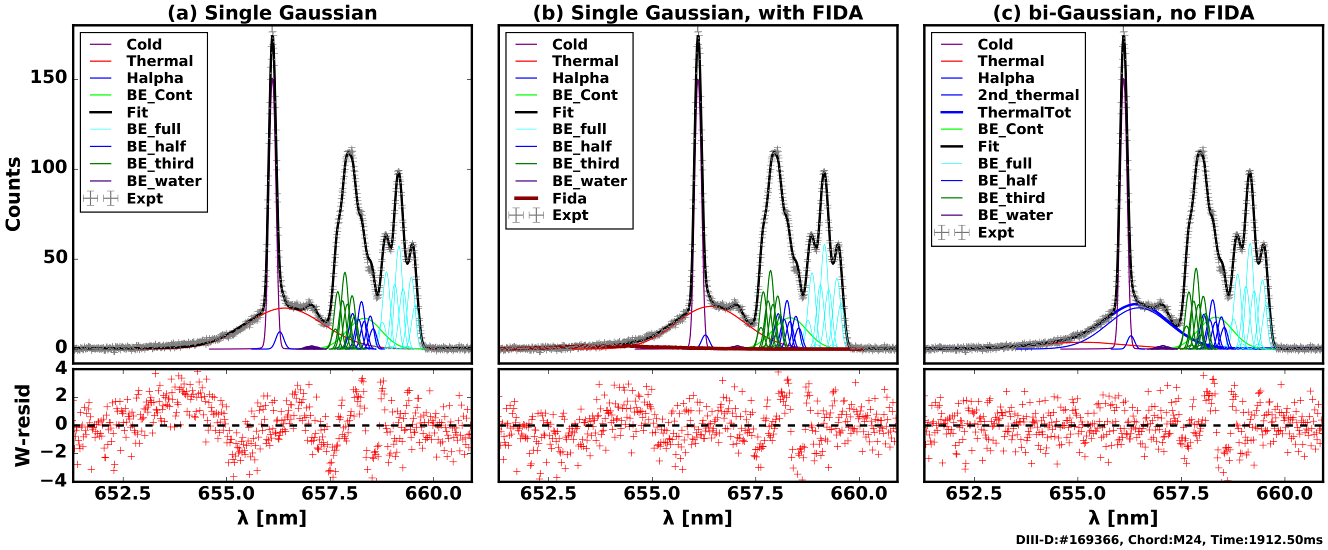

FIG. 5. Different fitting strategies for a particularly difficult spectrum from the QH-mode case. (a) Using a single Gaussian for the thermal component provides a poor fit which cannot account for the emission around 654 nm resulting in a weighted residual with significant structure. (b) Including the FIDA emission predicted by NUBEAM and FIDASIM in addition to the thermal Gaussian greatly improves the fit. (c) Excluding the FIDA emission but using two Gaussians to fit the thermal component. The resulting differences in the temperature and rotation measurements are shown in Fig. 6 (b) and (d).

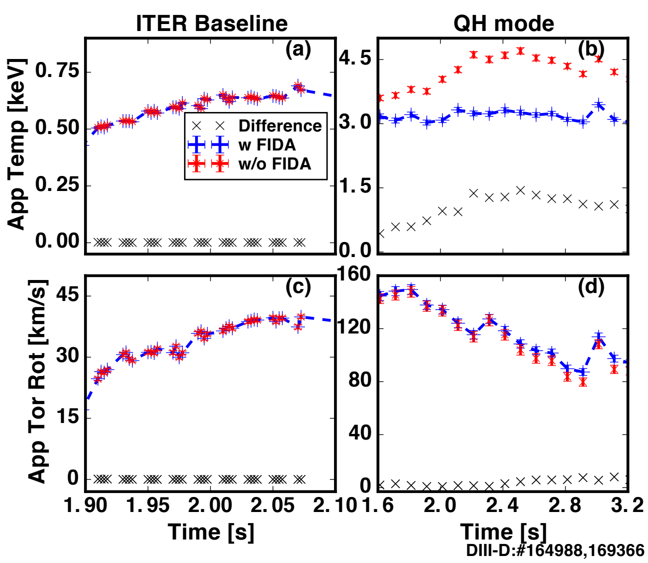

FIG. 6. Comparison between the bulk main ion temperature and rotation obtained for an ITER baseline case (a), (c) and a QH mode code (b), (d). Example spectra are shown in Figs. 3 and 5 for these two cases respectively.

of the thermal D_α emission. More specifically it gives the temperature, velocity, and radiance of the excited $n = 3$ deuterium neutral population that results from direct charge exchange (DCX) with neutral beams and subsequent charge exchange processes between the thermal neutrals and other thermal ions (halo). These processes mean that the $n = 3$ distribution function may contain distortions compared with the underlying D^+ thermal population which is why the measurements are referred to as "apparent". At the plasma edge, typically atomic cross section related distortions are minimal due to the lower ion temperature; however, the spatial smearing due to the halo and larger profile gradients becomes significant. On the other hand, in the core where temperatures are higher, the cross section distortions become important.

In order to convert these apparent values into the deuterium ion temperature, rotation, and density we need to model the process which leads to the excited $n = 3$ deuterium neutral population and the associated D_α emission based on the underlying plasma parameters. FIDASIM[24,25] is a Monte Carlo code which provides this functionality by calculating the density of multiple neutral deuterium populations (thermal, beam, fast) in several principle quantum states (collisional radiative modeling) on a 3D simulation grid as well as the associated D_α photoemission, using the following inputs: beam parameters, viewing geometry, EFIT equilibrium, electron density and temperature (n_e, T_e), deuterium ion temperature, angular rotation and density (T_D, Ω_D, n_D). A single impurity species is included with its density being calculated using n_e, n_D, the ion charge (Z_i) and assuming quasi-neutrality. FIDASIM provides a forward model of the measurement because it can calculate the spectrum for a particular sightline if the underlying deuterium properties are known. For details of the atomic physics data which is used in FIDASIM, see the references in 24 and 25.

The simulated apparent spectrum from FIDASIM is compared with the measured apparent spectrum for each sight line (Fig. 2 [c]) with the differences being used to generate a new set of deuterium ion input profiles for the next iteration of FIDASIM. This process is repeated until the simulated spectrum matches the observed spectrum at which point the input deuterium profiles provide the required deuterium ion properties which are consistent with the measured spectra. This iterative collisional radiative modeling is described in much greater detail in Refs. 14 and 13.

Currently the atomic physics modeling is the most time consuming part of the main ion analysis because each iteration of FIDASIM takes approximately 20 minutes. Ways that this process can be accelerated without significantly compromising accuracy are under investigation. One option is using the $n = 3$ neutral density from the first FIDASIM iteration with approximately correct main ion properties to calculate the emitted spectrum using different deuterium ion properties for subsequent iterations:

$$R(\lambda) \approx \frac{cA_{32}}{4\pi\lambda_0} \int_{LOS} n_3(l)\ f_M(T(l), v_d(l), \lambda)\ \mathrm{dl} \qquad (1)$$

where $R(\lambda)$ is the spectral radiance (Ph/sr/m^2/s/nm) as a function of wavelength (λ) along the line of sight, λ_0 is the D_α rest wavelength in nm, c is the speed of light, T and v_d are the plasma temperature and velocity projected onto the line of sight (these vary along the line of sight), A_{32} is the Einstein coefficient for the $n = 3 \rightarrow 2$ transition, n_3 is the density of excited $n = 3$ deuterium, and f_M is a Maxwellian distribution function. This removes the requirement to recalculate the neutral populations at each iteration step, reducing the time taken to calculate subsequent iterations from many minutes to less than a second each. However, any changes to the $n = 3$ density due to the changing deuterium ion properties between iterations are not included, nor is the fact that the neutrals carry the properties of their birth cell along with any atomic cross section distortions as opposed to the properties in the cell where the light is emitted. Initial tests show that this approach works well except near the separatrix where non local effects become important.

D. The fast ion D_α emission

An important difference between the main ion and impurity distribution functions in NBI or ICRH heated plasmas is the presence of a fast deuterium ion population. This population means that the deuterium distribution function is non-Maxwellian and the separation into a Maxwellian "thermal" bulk population and a "fast" population is somewhat arbitrary. The fast ion population also emits D_α light (FIDA)[22,26], so in cases where there is a significant fast ion fraction at the radius of the MICER measurements this emission must be treated carefully. This is usually a greater concern for the core main ion system[7] where the fast ion density is typically much larger. However, as we show in this section, for low density cases with high levels of NBI heating such as QH-mode, the fast ion contribution to the spectrum for the edge system must also be taken into account.

The approach that we take is to separate the fast and thermal ion population contributions to the MICER spectrum in a way that mirrors how they are separated in transport codes such as TRANSP[27]. The reason for doing this is that one of the main uses of the main ion measurements is in transport codes such as TRANSP, where they are used to calculate the thermal, momentum, and particle transport. In TRANSP, the NUBEAM[28] module calculates the birth profile of the fast ions (from charge exchange and ionization of the neutral beam particles). These particles are then followed as they transfer momentum and energy to the underlying "thermal populations" until their energy drops below $1.5T_i$ (where T_i is the Maxwellian thermal ion temperature) at which point they are added to the main ion thermal population. In this process the fast ions are essentially treated as a particle, momentum, and energy source for the thermal populations with the interaction between the populations being neoclassical.

An output of the NUBEAM calculation is the fast ion distribution function which can be used by the FIDASIM code to calculate the FIDA emission. This artificial FIDA spectrum is then used as one of the features in the fit to the main ion spectrum allowing the contribution of the fast ions to the spectrum to be properly accounted for, and the "thermal" population (according to the TRANSP definition) contribution to be properly extracted from the fit. This workflow is illustrated in Fig. 2 (a) and (b). This technique is limited to the extent that NUBEAM can accurately calculate the fast ion transport and FIDASIM can calculate the resulting FIDA emission for the MICER sight lines.

This approach differs from that taken in Ref. 15 where the thermal and fast parts of the distribution function are not artificially separated. Instead the temperature and rotation are calculated by taking moments using the full kinetic distribution function. While this is the kinetic temperature and rotation it would not be correct to use these values as inputs to TRANSP for interpretive transport because TRANSP is already including the effects of the fast ions separately.

For many cases the fast ion fraction near the plasma edge is low enough that the FIDA contribution to the spectrum can be neglected. This can be seen in the spectrum from the ITER baseline case shown in Fig. 3 where the FIDA radiance was calculated to be $\approx 0.1\%$ of the thermal radiance. Additionally, excluding the FIDA feature does not lead to significant patterns in the weighted residual (Fig. 3 [b]) whose values should be low and approximate random noise for a good fit.

To contrast against this case, a QH-mode case, which is one of the most challenging cases for MICER analysis on DIII-D, is shown in Fig. 5. Here the FIDA radiance was calculated to be ≈ 30% of the thermal radiance. When fitting the spectrum with a single Gaussian (Fig. 5 [a]) there is significant structure in the residual around 654 nm indicating a missing feature in the model (this structure is absent in Fig. 3). When the FIDA contribution is included (Fig. 5 [b]), the fit improves significantly. The remaining structure in the residual Fig. 5 (b) may be due to non-Maxwellian features in the "thermal" population itself[29,30]. For completeness, a fit including two separate Gaussians which absorb the contributions of the thermal and fast ion populations is shown in (c). While the fit is good, the interpretation is not as clear as directly including a modelled FIDA contribution because it is unknown how the contributions are absorbed into the two Gaussians and we do not have enough information from this number of view chords to unravel the complexities of the fast ion part of the main ion distribution function.

Fig. 6 compares the apparent temperature and toroidal rotation for both the ITER baseline ([a],[c]) and QH-mode case ([b],[d]) with and without including the FIDA feature in the fit to the spectra. For both fits, a single Gaussian is used for the thermal feature. The results for the ITER baseline case are essentially identical indicating that FIDA can be excluded for this particular chord; however, for the QH mode case, differences up to 1.3 keV (out of 3 keV) and 6km/s (out of 100 km/s) are seen demonstrating the importance of including the FIDA contribution when there is a large fast ion fraction.

This QH-mode is an example of one of the most difficult cases for MICER analysis that is enountered on DIII-D. More typical cases such as those shown in Fig. 3 can be fit with relative ease. These challenging cases provide an excellent opportunity to refine the MICER technique.

IV. EXAMPLE CAPABILITIES

In this section examples of profile measurements for the Ohmic and ITER baseline cases are shown, along with an example of the beam parameter measurements during a NBI variable beam perveance[31] control experiment which aimed to simultaneously control the input torque and stored energy.

Temperature and rotation profiles from the Ohmic case are shown in Fig. 7. This particular discharge was designed to study changes in the intrinsic toroidal rotation profile as the electron density is decreased. As was described in the introduction, improved understanding of intrinsic rotation is particularly important for larger machines such as ITER. Short beam blips (10ms) provide the MICER and CER measurements every 400ms. The main ion and impurity toroidal rotation profiles are shown in Fig. 7 (a) and (b) for the high density and low density times in the discharge respectively. The main ion rotation profile changes from hollow to almost flat as the density is decreased. One possibility for this change in profile is changes in the residual stress associated with changes in the dominant turbulence regime[32]. Comparing the impurity and main ion measurements, similar behaviour is seen for $\rho < 0.6$; however, for $\rho > 0.6$ the main ion rotation is essentially flat, while for the impurities it steadily decreases with increasing ρ (square-root of normalized toroidal magnetic flux). This clearly demonstrates the importance of the main ion measurements near the edge when studying topics such as intrinsic rotation.

The temperature profiles for these two cases are show in Fig. 7 (c) and (d). Both the deuterium and carbon temperatures are well equilibriated showing near identical values across the profile. The electron temperature is significantly higher in the core due to the Ohmic heating. Cases where there are significant differences between the main ion and impurity temperature are shown in Ref. 33.

The time evolution of the main ion and impurity toroidal rotation profiles for the higher powered ITER baseline case across the L-H transition, which occurs at 1896ms, are shown in Fig. 8. For $\rho < 0.7$ both the main ion and impurity toroidal rotation show similar increases. Near the separatrix significant differences between the rotation of the two species are seen. The impurity toroidal rotation develops a notch structure around $\rho = 0.93$ following the L-H transition which is often seen in the impurity toroidal rotation[34–36]. Additionally the main ion rotation shows a large co-current rotation near the separatrix which increases leading up to the L-H transition and a jump across the transition. This co-current edge peak has previously been observed using Mach probes[19]. Again, these profiles clearly show that the main ion measurements are crucial for understanding the plasma toroidal rotation near the plasma edge.

As was described in section III, the spectrally resolved beam emission component of the D_α spectrum contains a great deal of information about the neutral beams. Recent upgrades to the NBI and plasma control system (PCS) on DIII-D allow the beam voltage and perveance to be controlled in real time allowing for simultaneous control of the stored energy and toroidal rotation[31]. Recently feedback control of the stored energy and toroidal rotation by varying the beam voltage and current in the co and counter beams was attempted on DIII-D with the goal of enabling smoother, more precise control by avoiding beam modulations. Comparisons between the beam voltage and current reported by the NBI group (based on measurements inside the injectors) and the MICER measured beam voltage and full energy beam emission radiance (based on the Doppler shift and radiance of beam neutrals D_α emission as they travel through the plasma) are shown Fig. 9. Excellent agreement is seen with MICER capturing the time variation of the controlled values. The faster beam current variations were used to try to respond to fast changes in energy and/or rotation due to slower beam voltage response times. This further confirmes that the beam emission is being fit with a high degree of accuracy and demonstrates the utility of

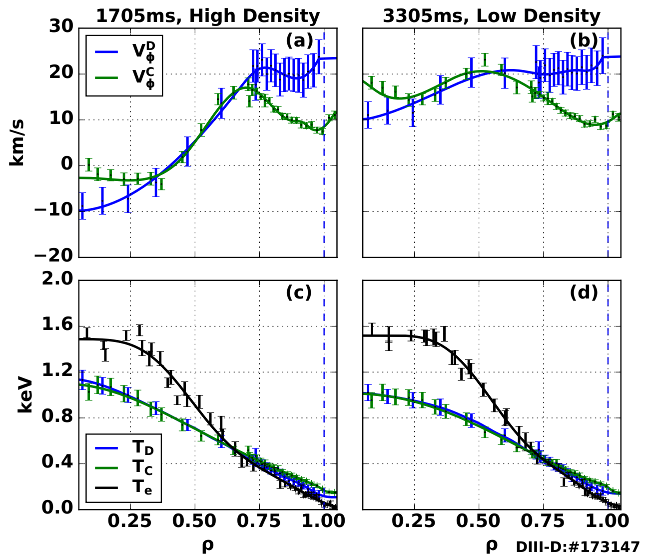

FIG. 7. Main ion and impurity toroidal rotation and temperature profiles for the Ohmic case at the high density (a),(c) and low density (b),(d) times. The profiles are plotted against the square root of the normalized toroidal flux (ρ).

the MICER system beyond measuring thermal main ion properties.

V. CONCLUSIONS AND FUTURE WORK

The main ion charge exchange recombination spectroscopy (MICER) system on DIII-D comprises 32 dedicated sight lines including a high resolution 16 channel edge system designed specifically to observe the main ion properties in the pedestal region. The difficulties encountered in performing MICER compared with impurity CER largely lie in the analysis of the spectrum and the required atomic physics modeling. Details of some of the advances which have allowed these measurements to be made from the plasma core to the edge have been described, in particular the iterative collisional radiative modeling required to account for the effect of the halo and atomic cross section distortions. The results from the timeslice subtracted spectra were shown to be robust to the choice of the background/passive time slice and the prospects of performing MICER without using time slice subtraction are promising inside the top of the pedestal, but errors of approximately 100 eV and 15 km/s are encountered near the separatrix. Including the FIDA emission was shown to be unnecessary for the majority of L-mode and H-mode cases for the edge main ion chords. However, for challenging cases such as QH-mode, including the FIDA emission is important for obtaining accurate measurements due to the low density, high temperature, and high fast ion fractions.

Time evolving profiles of the main ion properties from the core to the edge of the plasma were shown illustrating that large differences between the impurity and main ion toroidal rotation can occur, particularly near the plasma edge. This highlights the importance of the main ion measurements in research areas such as momentum transport. Additionally, the ability to accurately diagnose details of the neutral beam parameters based on the D_α light they emit was demonstrated.

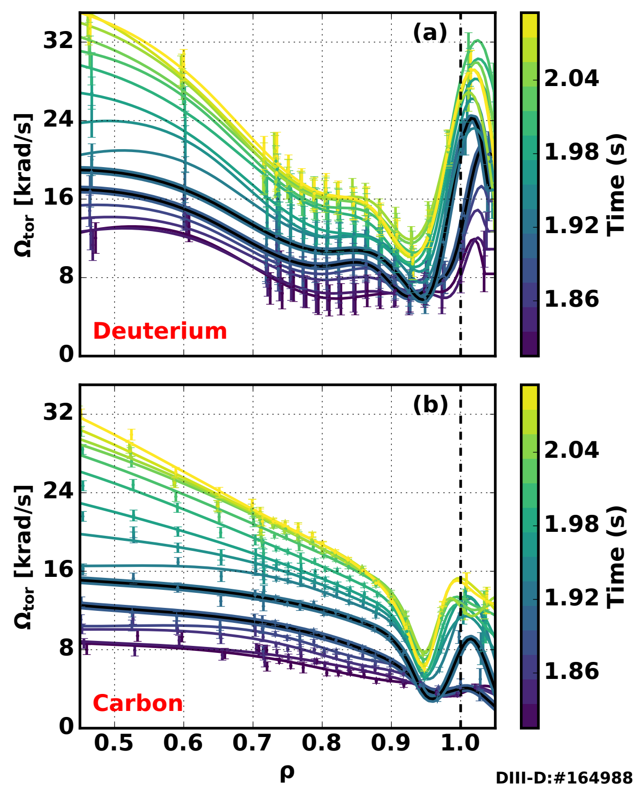

FIG. 8. Toroidal rotation profiles for the ITER baseline case across the L-H transition which occurs at 1896ms. The profiles on either side of the transition are marked with thicker colored lines and a thin black line. Large differences are seen - a rapid co current edge rotation is seen in the main ion profiles, and notch feature is seen for the impurity profiles. The dashed vertical line marks the separatrix.

Future work will focus on further reducing the time it takes to perform main ion CER analysis. Recent advances in the spectral fitting, which were described, have meant that between shot spectral fitting is possible; however, the iterative calculations which are required to account for spatial smearing due to the halo, and atomic cross section distortions are still time consuming. The 32 channel system has been acquiring data on most DIII-D discharges since 2016 providing a large database of main ion measurements over a broad range of plasma conditions which promises to provide a rich source of data for testing and further developing physics models.

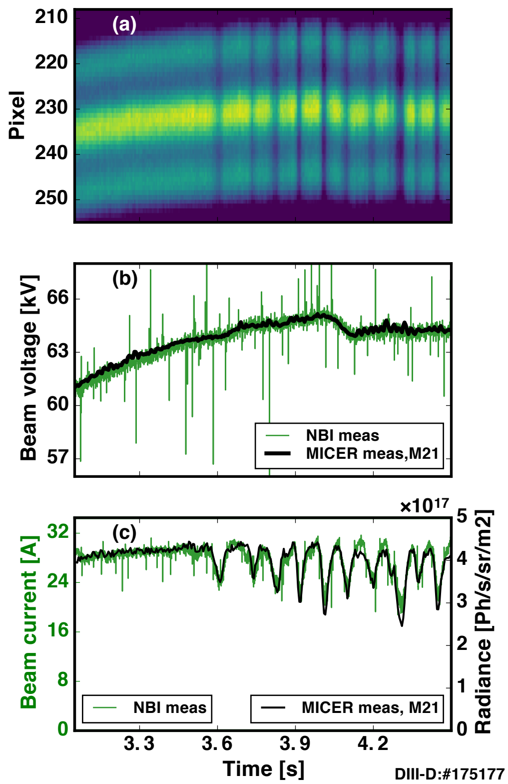

FIG. 9. (a) Time history of the full beam emission part of the D_α spectrum for main ion chord M21 during a beam perveance control experiment. The three separate peaks are due to the motional Stark effect splitting of the emission. (b) Comparison between the beam voltage measured at the NBI acceleration grid (green) and the beam voltage based on the measured Doppler shift of the beam emission in the D_α spectrum. (c) Comparison between the beam current as reported by the NBI group and the radiance of the full beam emission in the D_α spectrum. The radiance is proportional to the number of full energy beam neutrals.

VI. ACKNOWLEDGMENTS

This material is based upon work supported by the U.S. Department of Energy, Office of Science, Office of Fusion Energy Sciences, using the DIII-D National Fusion Facility, a DOE Office of Science user facility under Grants No. DE-AC02-09CH11466 (Princeton University), No. DE-FC02-04ER54698, and DE-FC02-95ER54309 (General Atomics). Portions of the data analysis were performed using the OMFIT integrated modeling framework[37] using the TRANSP[38] and OMFITprofiles[39] modules. DIII-D data shown in this paper can be obtained in digital format by following the links at https://fusion.gat.com/global/D3D_DMP.

VII. REFERENCES

[1] K. H. Burrell, Physics of Plasmas **4**, 1499 (1997).
[2] K. H. Burrell *et al.*, Physics of Plasmas **23**, 056103 (2016).
[3] R. J. Fonck, R. J. Goldston, R. Kaita, and D. E. Post, Applied Physics Letters **42**, 239 (1983).
[4] R. C. Isler, Plasma Physics and Controlled Fusion **36**, 171 (1994).
[5] R. J. Groebner, N. H. Brooks, K. H. Burrell, and L. Rottler, Applied Physics Letters **43**, 920 (1983).
[6] B. A. Grierson *et al.*, Nuclear Fusion **53**, 063010 (2013).
[7] B. A. Grierson *et al.*, Physics of Plasmas **19**, 056107 (2012).
[8] E. Berezovskij, M. Berezovskaya, A. Izvozchikov, V. Krupin, and V. Rantsev-Kartinov, Nuclear Fusion **25**, 1495 (1985).
[9] E. Busche, H. Euringer, and R. Jaspers, Plasma Physics and Controlled Fusion **39**, 1327 (1997).
[10] W. Mandl, Technical Report JET-IR(92)05, JET (1992).
[11] B. A. Grierson *et al.*, Review of Scientific Instruments **83**, 10D529(6) (2012).
[12] B. A. Grierson, K. H. Burrell, C. Chrystal, R. J. Groebner, S. R. Haskey, and D. H. Kaplan, Review of Scientific Instruments **87**, 11E545 (2016).
[13] S. R. Haskey, B. A. Grierson, K. H. Burrell, C. Chrystal, R. J. Groebner, D. H. Kaplan, N. A. Pablant, and L. Stagner, Review of Scientific Instruments **87**, 11E553 (2016).
[14] S. R. Haskey, B. A. Grierson, L. Stagner, K. H. Burrell, C. Chrystal, R. J. Groebner, A. Ashourvan, and N. A. Pablant, Journal of Instrumentation **12**, C10013 (2017).
[15] M. Salewski *et al.*, Nuclear Fusion **58**, 036017 (2018).
[16] V. A. Krupin *et al.*, Plasma Physics Reports **39**, 632 (2013).
[17] J. Kim, K. H. Burrell, P. Gohil, R. J. Groebner, Y. B. Kim, H. E. St. John, R. P. Seraydarian, and M. R. Wade, Physical Review Letters **72**, 2199 (1994).
[18] E. Viezzer *et al.*, Nuclear Fusion **55**, 123002 (2015).
[19] J. A. Boedo *et al.*, Physics of Plasmas **23**, 092506 (2016).
[20] M. Stejner *et al.*, Plasma Physics and Controlled Fusion **59**, 075009 (2017).
[21] C. Chrystal, K. H. Burrell, B. A. Grierson, S. R. Haskey, R. J. Groebner, D. H. Kaplan, and A. Briesemeister, Review of Scientific Instruments **87**, 11E512 (2016).
[22] W. W. Heidbrink, Review of Scientific Instruments **81**, 10D727 (2010).
[23] N. A. Pablant, K. H. Burrell, R. J. Groebner, C. T. Holcomb, and D. H. Kaplan, Review of Scientific Instruments **81**, 10D729 (2010).
[24] W. W. Heidbrink, D. Liu, Y. Luo, E. Ruskov, and B. Geiger, Communications in Computational Physics **10**, 716 (2011).
[25] L. Stagner, "FIDASIM code repository, https://github.com/D3DEnergetic/FIDASIM," (2016).
[26] Y. Luo, W. W. Heidbrink, K. H. Burrell, D. H. Kaplan, and P. Gohil, Review of scientific instruments **78**, 033505(11) (2007).
[27] R. Hawryluk, in *Physics of Plasmas Close to Thermonuclear Conditions* (Elsevier, 1981) pp. 19–46.
[28] A. Pankin, D. McCune, R. Andre, G. Bateman, and A. Kritz, Computer Physics Communications **159**, 157 (2004).
[29] D. J. Battaglia *et al.*, Physics of Plasmas **21** (2014), 10.1063/1.4886803.
[30] D. J. Battaglia *et al.*, Plasma Physics and Controlled Fusion **58**, 085009 (2016).
[31] D. Pace *et al.*, Nuclear Fusion **57**, 014001 (2017).
[32] B. A. Grierson *et al.*, Physical Review Letters **118**, 015002 (2017).
[33] S. R. Haskey, B. A. Grierson, and C. Chrystal, Manuscript submitted for publication with Plas. Phys. Control. Fus. (2018).
[34] D. R. Ernst *et al.*, Physics of Plasmas **5**, 665 (1998).

[35]T. Pütterich, E. Wolfrum, R. Dux, and C. F. Maggi, Physical Review Letters **102**, 025001 (2009).
[36]J. S. DeGrassle, K. H. Burrell, L. R. Baylor, W. Houlberg, and J. Lohr, Physics of Plasmas **11**, 4323 (2004).
[37]O. Meneghini *et al.*, Nuclear Fusion **55**, 083008 (2015).
[38]B. A. Grierson *et al.*, Fusion Science and Technology **00**, 1 (2018).
[39]N. C. Logan *et al.*, Fusion Science and Technology **00**, 1 (2018).